Tropopause region temperatures and CFC 11 mixing ratios from CRISTA 2

V. Kuell,[1,2] D. Offermann,[1] M. Jarisch,[1] B. Schaeler,[1,3] A. Engel,[4] H. Claude,[5] H. G. J. Smit,[6] A. Ebel,[7] and H. Feldmann[7]

Received 9 November 2004; revised 18 May 2005; accepted 9 June 2005; published 20 August 2005.

[1] Nearly global measurements of CFC 11 ($CFCl_3$) in the upper troposphere and stratosphere are presented. Data are from the CRyogenic Infrared Spectrometers and Telescopes for the Atmosphere (CRISTA 2) experiment in August 1997. They are the first global CFC 11 data set that covers the altitude regime 8 km to 28 km. A new temperature data product was developed for the CFC 11 retrieval by combining high accuracy of UKMO temperatures with high spatial resolution of CRISTA temperatures. At midlatitudes these temperatures and resulting CFC 11 mixing ratios are compared to in situ measurements and the regional CTM system EURAD. Measured temperatures agree within about 1 K (except at the cold point tropopause). CFC 11 mixing ratios agree within 0–15%, depending on altitude. Model temperatures of EURAD have a small warm bias (1 K). Model CFC 11 has a low bias of 15–30 pptv (10% at 147 hPa). The high resolution transport model data are for the first time combined with dense and reliable CFC 11 measurements from space to study specific dynamical features. Emphasis is on a midlatitude blocking event characterized by an omega circulation pattern with a persistent cutoff low at its western wing. At low latitudes our CFC 11 mixing ratios and temperatures suggest a warm bias of the UKMO temperatures near the tropical tropopause.

Citation: Kuell, V., D. Offermann, M. Jarisch, B. Schaeler, A. Engel, H. Claude, H. G. J. Smit, A. Ebel, and H. Feldmann (2005), Tropopause region temperatures and CFC 11 mixing ratios from CRISTA 2, *J. Geophys. Res.*, *110*, D16104, doi:10.1029/2004JD005592.

1. Introduction

[2] The atmospheric region a few kilometers above and below the tropopause is a regime of strong and important dynamical, photochemical, and energetic processes. Much scientific interest has especially focused on the upper troposphere/lower stratosphere (UT/LS) region, sometimes dubbed the ''middle world''. It is defined as the region wherein isentropic surfaces do not lie entirely in the stratosphere, nor do they intersect the earth surface layer [e.g., *Holton et al.*, 1995; *Shepherd*, 2002]. Material exchange between the troposphere and the stratosphere is an important objective of research for a number of reasons, and it occurs in this atmospheric layer. Generally speaking, transport through the UT/LS region is mainly directed upwards in the tropics and mainly downwards in the extratropics (Brewer–Dobson circulation).

[3] The tropopause is frequently considered to be a transport barrier [e.g., *Haynes and Shuckburgh*, 2000; see also *Schaeler et al.*, 2005, and references therein]. It needs to be noted, however, that it is a barrier only for turbulent (mixing) transports, and that this barrier is not impermeable, but it is leaky. Local or regional cross-tropopause transports appear to be associated with disturbances of the tropopause, i.e. deviations from its large scale ''smooth'' shape. There are many different types of such disturbances, as for example tropopause folds [e.g., *Elbern et al.*, 1998; *Sprenger et al.*, 2003], cutoff lows [e.g., *Ancellet et al.*, 1994; *Feldmann et al.*, 2003], blocking events [e.g., *Benzi et al.*, 1986; *Fournier*, 2003; *Pelly and Hoskins*, 2003], and horizontal intrusions from the stratosphere into the troposphere [*Appenzeller and Davies*, 1992; *Ebel et al.*, 1991; *Elbern et al.*, 1997; *Waugh and Polvani*, 2000; *Waugh and Funatsu*, 2003; *Saraf et al.*, 2003].

[4] Blocking systems occurring within the latitude belt of baroclinic westerlies effectively reduce zonal transport of atmospheric properties and enhance meridional exchange in the troposphere and lower stratosphere. They are persistent dynamical features and last over several days, sometimes even weeks. They are most frequently observed in late spring and least frequently in late summer. Three major types may be identified: high-over-low blocks (sometimes called Rex blocks [*Rex*, 1950]), omega blocks and stationary high amplitude ridges. The first type forms a dipole structure with a pronounced ridge on the poleward side and

[1]Physics Department, University of Wuppertal, Wuppertal, Germany.
[2]Now at Meteorological Institute, University of Bonn, Bonn, Germany.
[3]Now at CETEQ, Wuppertal, Germany.
[4]Institute for Meteorology and Geophysics, University of Frankfurt, Frankfurt, Germany.
[5]Meteorological Observatory, Hohenpeissenberg, Germany.
[6]ICG–2, Research Center Juelich, Juelich, Germany.
[7]Rhenish Institute for Environmental Research, University of Cologne, Cologne, Germany.

0148-0227/05/2004JD005592

a trough on the equatorial side, causing anomalous easterlies between them in a region where usually westerly flow is prevailing. The omega structure is characterized by a central ridge with cyclonic systems at its left and right side, so that the flow around the blocking ridge follows the shape of the Greek character Ω. The cyclonic pressure systems may exhibit the characteristics of a cutoff low (COL), meaning that the core of the trough has closed streamlines and height contours. On the northern hemisphere increased blocking activity is found over the west coast of North America and Europe. Yet specific features of the climatology depend on the method applied to the identification of blocking events [*Sausen*, 1995]. Also many details of the dynamical processes controlling the life cycle of blocking events are not yet completely understood.

[5] COLs which are much more frequent than blocking events are generated when troughs in the upper level westerlies are disconnected from the polar vortex leaving an isolated cyclonic system with polar air mass on the equatorial side of the jet stream. If a COL does not reconnect with the polar vortex the polar air masses will finally be mixed with midlatitude air. This shows the relevance of COLs for meridional transport. In the case of omega blocks meridional transport occurs in both directions, towards higher and lower latitudes on the western and eastern flank of the central high, respectively. In COLs and pronounced troughs the tropopause height is, sometimes dramatically, decreased below average whereas it is slightly increased in ridges causing enhanced exchange of stratospheric and tropospheric air with net transformation into tropospheric air in cyclonic systems and into stratospheric air in anticyclonic ones. In the UTLS concentrations of trace gases are modified by the dynamic systems. For instance, ozone mixing ratios, which are increasing vertically and/or poleward, are enhanced/reduced in the cyclonic/anticyclonic structures. These changes are negatively correlated with changes of trace gas mixing ratios like those of water vapor, which shows vertical and latitudinal gradients opposite to those of ozone.

[6] A region of special importance and complexity is the tropical tropopause. It has become increasingly clear in recent years that it is not the thermal tropopause (at 16–17 km) that plays the decisive role in linking the troposphere and the stratosphere, but rather an extended region instead [*Shepherd*, 2002]. Tropospheric Hadley circulation and convection reaches up to about 12 km, a level which is sometimes called the secondary tropopause. Above an altitude level of 14 km convective overturning strongly decreases, and a mixing barrier even has been defined by *Folkins et al.* [1999] at this level. The same level was denoted as the chemopause by these authors, as photochemistry is considerably reduced below this altitude. The regime between the thermal tropopause and the secondary tropopause (or the chemopause) is sometimes called the Tropical Transition Layer (TTL) or simply the Tropical Tropopause Layer (TTL) [*Shepherd*, 2002]. Frequently, however, a larger vertical regime is assumed for the TTL, namely from the Level of Neutral Buoyancy (LNB) at about 150 hPa (14 km) to the Level of Maximum Overshoot (LMO) at about 50 hPa (19 km) [*Sherwood and Dessler*, 2000, 2001]. Here the LMO is the highest altitude reached by overshooting convective updrafts.

[7] For the experimental study of the lower stratosphere and upper troposphere one needs data sets of dynamical parameters and trace gas mixing ratios with high spatial resolution and large coverage in a sufficient altitude regime. High spatial resolution can be achieved by balloon and aircraft measurements on flight trajectories. Balloons, radiosondes and ozonesondes yield data at high vertical resolution [e.g., *Engel et al.*, 1997; *Fabian and Borchers*, 2001; *Folkins et al.*, 2002; *Voemel et al.*, 2002]. As regards aircraft measurements they have high horizontal resolution and relatively large coverage in one dimension [e.g., *Elkins et al.*, 1996; *Marenco et al.*, 1998; *Sherwood and Dessler*, 2000; *Tuck et al.*, 2004, and references therein]. They tend to concentrate on specific altitude levels.

[8] Remote sensing measurements of various parameters can be active or passive, and can be taken from the ground, airplane, balloon, and satellite [e.g., *Fujiwara et al.*, 2003; *Heese et al.*, 2001; *Lait et al.*, 2002; *Toon et al.*, 1999; *Chang et al.*, 1996; *Bingham et al.*, 1997; *Roche et al.*, 1998]. The suborbital measurements have, as discussed above, various specific merits. They are, however, rather localized in space and time. The satellite measurements have the advantage of (nearly) global coverage and (mostly) long duration. Their spatial resolution is, however, fairly limited, especially if occultation measurements are considered. Moreover, data taking in the lowest stratosphere and middle to upper troposphere is difficult for many of the satellite experiments.

[9] In the present paper we present CRISTA satellite data which have a much increased spatial resolution [*Offermann et al.*, 1999; *Grossmann et al.*, 2002]. In addition, the vertical data coverage has been increased, and data are now available above 8 km in the troposphere and in all of the stratosphere (and mesosphere). We here restrict our analysis to altitudes of 8 km to 28 km. We have analyzed temperatures and several trace gases in this altitude regime. We have chosen CFC 11 as the trace gas especially suitable for transport studies, as it has a steep vertical mixing ratio profile and a simple photochemistry at these altitudes. Results of temperature and CFC 11 mixing ratios are given in the present paper. Mixing ratios of water vapor and ozone are given in the companion paper by *Schaeler et al.* [2005]. Eddy transports derived from the three gases are also given in that paper. The trace gas data are discussed in comparison with the regional high resolution European Air Pollution Dispersion (EURAD) model. (For a short description of the EURAD model system, see section 2.3.)

[10] CFC 11 data have been measured in the infrared by the Atmospheric Tracer Molecule Spectroscopy (ATMOS) experiment during several Space Shuttle flights. *Chang et al.* [1996] report corresponding results from measurements during the ATMOS/ATLAS 3 mission at northern midlatitudes and southern high latitudes. The ATMOS experiment used the solar occultation technique, and hence the spatial resolution of the data is rather limited. During another Space Shuttle flight the Cryogenic Infrared Radiance Instrumentation for Shuttle (CIRRIS) experiment took infrared emission measurements of CFC 11 at several latitudes and longitudes. A rather limited number of altitude profiles

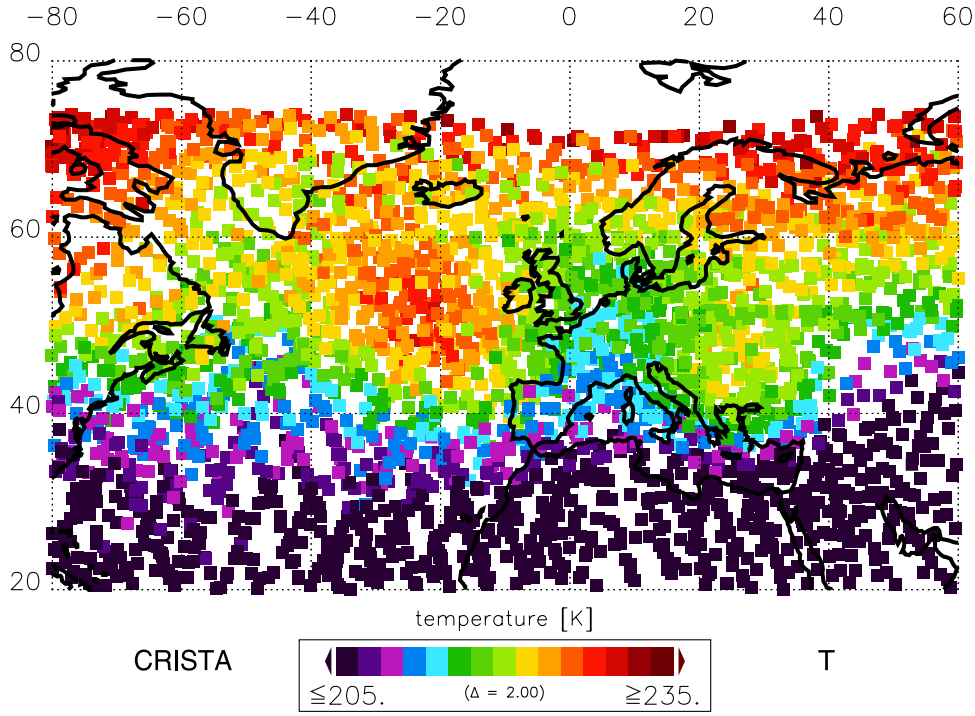

Figure 1. CRISTA-UKMO-Combined (CUC) temperatures at 16 km (≈100 hPa) altitude in the TRACHT area. Data are shown for the time interval 10–13 August 1997. Each dot stands for one temperature altitude profile (CRISTA vertical scan). (Values higher than the upper limit or lower than the lower limit of the color code are colored in dark red and dark violet as denoted by the arrows.)

have been published by *Bingham et al.* [1997]. Extended measurements of infrared emissions were performed by the UARS Cryogenic Limb Array Etalon Spectrometer (CLAES). Corresponding mixing ratios of CFC 11 have been retrieved and presented only in the middle stratosphere, i.e. above 20 km [*Roche et al.*, 1998]. Hence the CFC 11 mixing ratios presented here are, to our knowledge, the first near global data set at high spatial resolution which covers the upper troposphere and the lower stratosphere.

[11] The paper structure is as follows: In section 2 the "CRISTA-UKMO combined" (CUC) temperatures are introduced as a new data product. These temperatures are a combination of CRISTA temperatures and UKMO temperatures [*Swinbank and O'Neill*, 1994]. They are used to retrieve the CFC 11 data. The generation of the temperature data set and its measurement errors are described and the temperature distribution on regional scales is shown. The CUC temperatures are compared to radiosonde and airborne measurements, and the temperature variability is investigated. Subsequently the CUC temperatures are compared to results of the EURAD model. In section 3 the CRISTA CFC 11 data are compared to other CFC 11 measurements in regional areas. Subsequently it is shown that this data product is very useful for the analysis of dynamical structures (a Cutoff Low (COL) and a blocking event in the area). Furthermore the measurements are compared to the results of the EURAD model with special emphasis on small scales and data variability. In section 4 the global distribution of measured CFC 11 data is presented. Discussion and Conclusions sections follow.

2. Regional Temperature Analysis

2.1. Measurements

[12] Temperature measurements have been analyzed in a specifically chosen region, the so-called TRACHT area, a region of the North Atlantic and west Europe where a special TRAnsport, CHemistry and Trace gas study has been conducted [see *Feldmann et al.*, 2003; *Offermann et al.*, 2003] during the time period of the CRISTA mission. Other measurements are from 16 radiosondes released at the Hohenpeissenberg station (48°N, 11°E), and from the airborne MOZAIC instruments [*Marenco et al.*, 1998; *Helten et al.*, 1998] on 13 flights across the Atlantic.

[13] CRISTA measured temperatures in the middle atmosphere during its second mission (7–19 August 1997). The limb-scan measurements were found to be biased below 20 km altitude, when compared to radiosondes (at Hohenpeissenberg and other stations [*Lehmacher and Offermann*, 1997]). To correct for this bias, the data were combined with UKMO temperatures in the following way: CRISTA and UKMO mean temperatures were calculated in latitudinal bands of 5° width. The temperature bias was determined with UKMO as a reference, and the bias was subsequently used to correct all CRISTA temperatures in this latitudinal band. This procedure was applied to all latitudes and altitudes used in the present analysis. We call this data

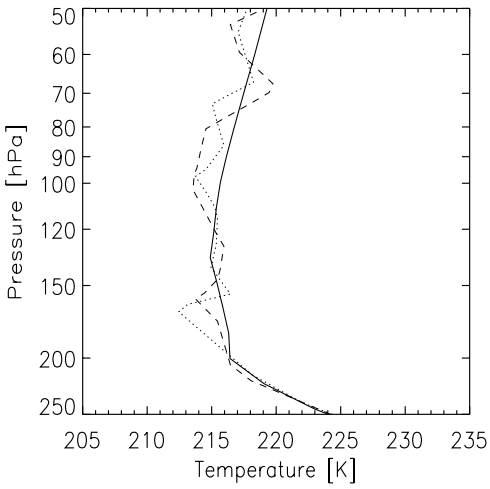

Figure 2. Comparison of radiosonde and CUC temperatures. Two radiosondes released from Hohenpeissenberg at 08:27 UT (dotted) and 11:34 UT (dashed), respectively, on 12 August 1997. Mean of 8 CUC profiles measured on 12 August 1997 near Hohenpeissenberg (solid line) ($\leq \pm 3°$ longitude and latitude, see text).

set the CRISTA-UKMO-Combined (CUC) temperatures. An example is given in Figure 1 for the altitude of 16 km ($\approx$100 hPa). The CUC temperature absolute accuracy thus is the same as that of the UKMO temperatures. The precision is that of CRISTA, i.e. 0.3 K at 16–20 km, and 0.4 K at 12–14 km. These values are upper limits. The horizontal resolution of the CUC temperatures is that of the CRISTA measurements (e.g., Figure 1). The vertical resolution is also that of CRISTA (2 km). There appears to be still an accuracy problem with the tropical temperatures (TTL area) which is discussed below.

2.2. Measurement Intercomparisons

[14] To check the consistency of the three measured temperature sets, a few intercomparisons are performed. Figure 2 shows two radiosonde ascents on 12 August 1997 (day of year (DOY) 224) together with a CUC mean profile. Absolute accuracy and precision of the radiosonde temperatures are ±0.5 K each [*Yagi et al.*, 1996; *Luers and Eskridge*, 1998]. The mean profile in Figure 2 was computed from eight individual profiles measured on that day in the neighborhood of Hohenpeissenberg (±3° longitude, ±3° latitude). We performed three more intercomparisons of this type (DOYs 222, 223, 225), which all look like Figure 2. The CUC profile in Figure 2 is found to be in reasonable agreement with the two radiosonde profiles, if one ignores the fluctuations or wavelike structures seen in these latter data. The CRISTA vertical profiles, and thus those of the CUC data, are not suitable for detecting small scale waves with small horizontal/vertical wavelengths because CRISTA integrates emissions along its line-of-sight over approximately 250 km [*Preusse et al.*, 2002]. Because of this and because a mean of eight profiles was taken the CUC profile in Figure 2 looks very smooth. More details are shown in Figure 3. This picture gives the deviations of the eight radiosonde profiles from their common mean (Figure 3a). Figure 3b shows the standard deviations from that mean. They are appreciable especially in the lower part of the altitude regime, i.e. around the tropopause altitude. Similar diagrams are shown for 32 CUC profiles in Figures 3c and 3d. It can be seen that there are notable vertical structures in the CUC data, too, but not at the very small scales as with the radiosondes. The temperature variations mostly represent atmospheric fluctuations given the instrument precisions cited. The difference between the mean CUC profile and the radiosonde mean profile is shown in Figure 3e. A close agreement is found except at the altitudes of the "cold point tropopause" (point of lowest temperature), which is difficult to detect for a limb scanning instrument like CRISTA.

[15] Generally a positive bias of the CUC temperatures is indicated in Figure 3e. It is, however, fairly small, i.e. on the order of 1 K, and thus within the combined error bars. It is considerably smaller than the fluctuations (standard deviations) shown in Figures 3a–3d, especially at the lower altitudes. The strong variations at around 200 hPa are believed to be due to strong fluctuations of the tropopause altitude. This is supported by calculations of the EURAD model, which show a highly variable tropopause height near this station [*Feldmann et al.*, 2003, Figures 7–13]. More details are given by *Offermann et al.* [2003; see also *Schaeler et al.*, 2005].

[16] Horizontal profile can be studied by means of the airplane data. A comparison of 13 horizontal profiles measured by MOZAIC during 13 transatlantic flights and the respective CUC temperatures was performed. Cruise altitude was near 220 hPa. Miss distance and miss time of CRISTA and MOZAIC measurements were 500 km and six hours, respectively. These values have been chosen fairly large in order to obtain a sufficient number of data points. The mean difference of the CUC and MOZAIC temperatures obtained is very small: −0.03 K (CUC minus MOZAIC). Thus almost perfect agreement is obtained. A difference this small must, of course, be fortuitous to some extent, as its standard deviation is large: σ_d = 4.54 K. Details are given by *Offermann et al.* [2003].

2.3. Description of the EURAD Model

[17] Atmospheric structure and development have been modeled by means of the EURAD system. This was mostly done in a regional analysis in the North Atlantic and Western Europe TRACHT area and time. The EURAD system consists of a meso-scale meteorological model (MM5 [*Grell et al.*, 1995]), the EURAD CTM (with the RADM2 chemical mechanism [*Stockwell et al.*, 1997] adjusted to tropopause region conditions) and the EURAD emission model [*Memmesheimer et al.*, 1991]. The calculations have been carried out for 29 layers covering the height range between the Earth's surface and 10 hPa. ECMWF global analyses were used for defining meteorological boundary and initial conditions. Details are presented by *Feldmann et al.* [2003]. The horizontal resolution of the EURAD model is 54 km, as compared to 250 km for the CRISTA measurements. We compare our measured data to the EURAD results for temperature and CFC 11. This way we mutually check on the reliability of the measured and modeled data, especially on small scales. We eventually use the EURAD results on the smallest scales

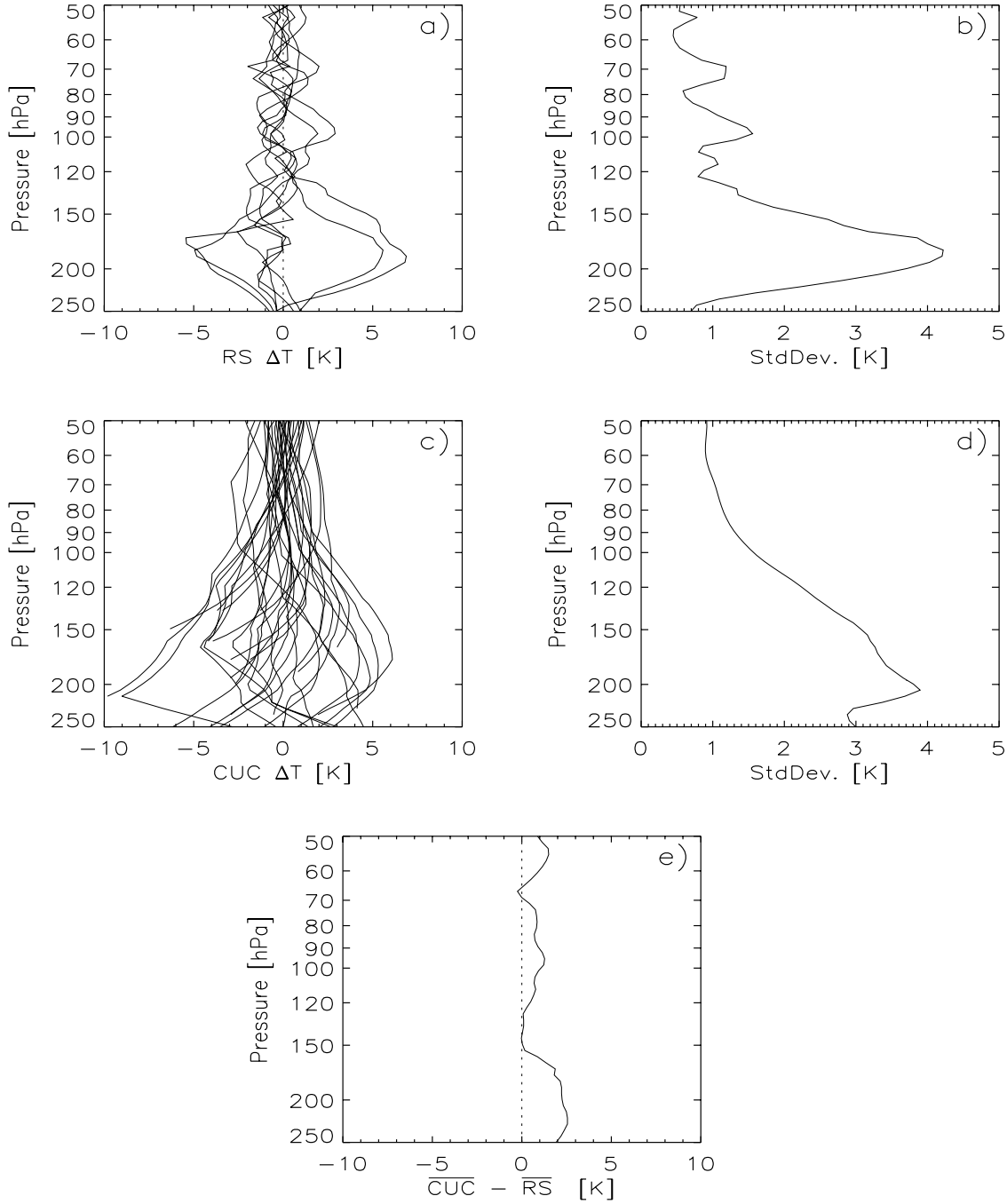

Figure 3. Temperatures at Hohenpeissenberg. (a) Deviations of eight radiosonde measurements from their mean (two launches per day on DOY 222–225, 1997). (b) Standard deviations for Figure 3a. (c) Deviations of 32 CUC temperature profiles from their mean (see text). (d) Standard deviations for Figure 3c. (e) Difference of CUC and radiosonde mean profiles.

not accessible to our measurements in our companion paper [*Schaeler et al.*, 2005].

2.4. Comparison of Measured and Modeled Temperatures

[18] EURAD model temperatures were mainly compared to our CUC temperatures, but furthermore to in situ measurements by radiosondes and airplanes (MOZAIC). Mean temperature differences of CUC and EURAD have been calculated for five pressure levels between 75 hPa and 225 hPa. A small positive bias of the EURAD temperatures of 0.63 K is obtained, with little altitude variations. Comparison of EURAD with the other measurements (radiosondes and MOZAIC) also shows a positive EURAD bias. It is, however, relatively small. (For details, see *Offermann et al.* [2003].) It is therefore concluded that the EURAD temperatures can be quite reliably used for atmospheric structure analyses.

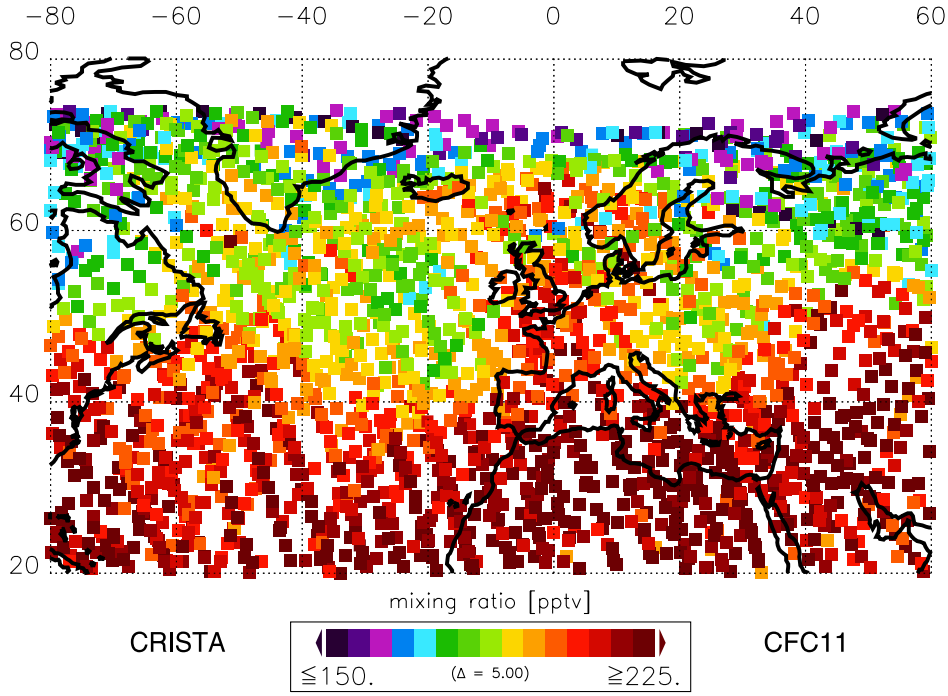

Figure 4. CFC 11 distribution at 100 hPa (≈16 km) in the TRACHT area as measured by CRISTA 2 during 10–13 August 1997.

[19] Atmospheric variabilities of the model have been compared to the measurements by *Offermann et al.* [2003]. This includes a study of spatial differences by means of structure functions. It can be concluded that the EURAD model reproduces the atmospheric temperature variability reasonably well.

3. Regional CFC 11 Analysis

3.1. CFC 11 Measurements

[20] In the upper troposphere and lower stratosphere CFC 11 is neither involved in fast gas phase/heterogeneous chemistry nor can it undergo any phase transitions. CFC 11 has its only source at the ground and is then transported into the stratosphere, where it is photolyzed at higher altitudes. In the troposphere, the photochemical lifetime is up to over 100 years, and decreases very strongly with increasing altitude. The resulting very steep gradient of mixing ratio in the stratosphere makes CFC 11 an excellent tracer to analyze dynamics in the UTLS region. The standard CRISTA 2 version 1 data set contains CFC 11 fields with an altitude coverage from 15 to 28 km. The standard retrieval method for CRISTA trace gas data is described by *Riese et al.* [1999a]. To extend this data set down to the lowermost altitudes CRISTA is able to measure, an improved retrieval algorithm was set up. CFC 11 mixing ratios were retrieved from the 11.8 μm emission band, and the CUC temperatures were used (instead of CRISTA 2 V1 temperatures) as input for the trace gas retrieval. The resulting global CFC 11 data set is analyzed in the present paper. It covers the altitude region from 28 km down to about 11 km in the standard measuring modes, and to about 8 km in a special measuring mode. (For details of the CRISTA 2 mission, see *Grossmann et al.* [2002].) Figure 4 shows a map of these CFC 11 data in the TRACHT area [*Offermann et al.*, 2003; *Feldmann et al.*, 2003] at 100 hPa (≈16 km). It corresponds to the temperature map in Figure 1.

[21] The accuracy of the trace gas mixing ratios has been estimated from retrieval simulations. (For details, see *Riese et al.* [1999a].) As mentioned, the input temperatures used for the retrieval of the CFC 11 data presented here are the CUC temperatures. Thus, the accuracy of the CFC 11 mixing ratios depends on the accuracy of UKMO temperatures. An upper limit of the systematic error of UKMO temperatures can be estimated conservatively from a comparison with radiosondes by *Manney et al.* [1996], who found differences on the order of 0.5–1.8 K. The resulting accuracy of CFC 11 mixing ratios is estimated to be better than 6–8% at 12–18 km and 8–10% at 20 km at low and mid latitudes. Towards higher latitudes and altitudes the values in percent tend to increase. Estimated upper limits for the precision are 1.8% at 12 km, 0.7% at 15 km, and about 6% at 24 km altitude. The error of the UKMO temperatures, and hence of the CFC 11 data, appears to be greater than quoted in the tropics (TTL regime). This is discussed in section 4.

3.2. Measurement Comparisons

[22] The CFC 11 mixing ratios are compared with both in situ and remote measurements from aircraft and balloon-borne instruments. From samples collected by the balloon borne cryogenic whole air sampler BONBON [*Schmidt et al.*, 1987; *Engel et al.*, 1997] a mean profile is derived for summer 1997. To do this, BONBON measurements from different years have been combined. The atmospheric trends are removed from the observations using the tropospheric trends derived from the NOAA/CMDL network [e.g.,

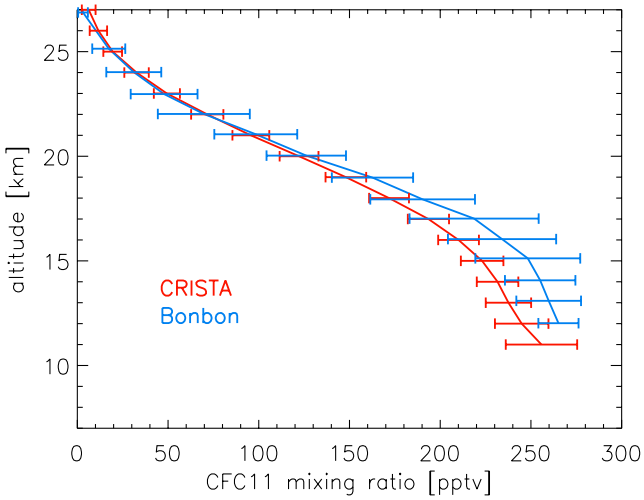

Figure 5. Comparison between CRISTA CFC 11 (red, all CRISTA data averaged over the region 39–49°N, 30°W–30°E) and an inferred CFC 11 profile for mid 1997 obtained from BONBON measurements (blue). For details, see text.

Montzka et al., 1999]. The propagation of tropospheric trends into the stratosphere is calculated in the same way as described in *Engel et al.* [2002]. This procedure is only valid for gases which are conserved during the transport in the stratosphere. In order to apply this procedure to CFC 11 measurements, an apparent age has been used in the trend calculations, based on the parameterization given by *Plumb et al.* [1999]. In this way all observations have been detrended and again retrended in order to be representative for mid 1997. Seven balloon flights have been used for the calculation of the CFC 11 profile (five flights from Aire sur l'Adour (44°N, 0°E) on 5 November 1990, 10 November 1990, 20 September 1993, 10 October 2001, 24 September 2002, and two flights from Gap-Tallard (44°N, 6°E) on 26 June 1991 and 23 June 1997.) The CFC 11 measurements by BONBON are given on the NOAA/CMDL mixing ratio scale [e.g., *Elkins et al.*, 1993], which has an absolute accuracy of 1% (J. Elkins, NOAA/CMDL, private communication). The measurement uncertainty for the CFC 11 mixing ratios was about 5% in 1990 and has been improved to less than 1% for observations since 2000. The mixing ratios derived after detrending and retrending to 1997 were binned according to geopotential altitude (1 km intervals), averaged and the resulting profile was smoothed using a 3 km running mean.

[23] Figure 5 shows the balloon CFC 11 profile calculated for summer 1997 obtained from BONBON and the corresponding mean CRISTA profile (averaged over the region 39–49°N, 30–30°E). Excellent agreement is obtained in the stratosphere, and in the troposphere both profiles agree well within their combined scatter bars. (The scatter bars essentially show the atmospheric variability.) The CRISTA CFC 11 mixing ratios appear to be somewhat lower than the balloon data at the lowermost altitudes.

[24] Next we compare CRISTA CFC 11 with measurements both from the Jet Propulsion Laboratory MkIV interferometer and the ACATS IV experiment aboard the NASA ER-2 aircraft (data from Plate 3 of *Toon et al.* [1999]). Both experiments measured during the Photochemistry of Ozone Loss in the Arctic Region in Summer (POLARIS) campaign in April/May 1997. This means that long term trends in CFC 11 can be neglected for the comparison with CRISTA (August 1997), but the result is more dependent on the specific meteorological situation during the aircraft/balloon flights. The aircraft measurements were made between April 30 and May 11, 1997 and the balloon profile was taken on May 8, 1997, all near Fairbanks, Alaska within the region 63–72°N, 141–157°W. The comparison with CRISTA CFC 11 is shown in Figure 6. The (black and red) error bars give the absolute errors in this picture.

[25] *Toon et al.* [1999] attribute the high variability of the ACATS IV data to different histories of the air masses encountered near Fairbanks. Considering this variability within the ACATS IV data, the dynamic activity suggested by the MkIV profile, and the difference in the time of the measurements (3–4 months), the mean CRISTA CFC 11 profile is in reasonable agreement with ACATS IV and MkIV.

3.3. Horizontal and Vertical Structure

[26] Figure 7 shows the horizontal CFC 11 distribution obtained by CRISTA over the Atlantic and Europe at 147 hPa (≈14 km) on one day. Tropospheric air is situated at low latitudes and stratospheric air at higher latitudes. Obviously, the transition from tropospheric air (color coded in red) to stratospheric air (color coded in blue and below) is horizontally highly structured. A prominent structure in this region is an omega blocking structure over the Atlantic and western Europe (thin black line in Figure 7). It is associated with a cutoff low (COL) located west of Ireland and south of Iceland. The COL contains air of stratospheric origin, which is poor in CFC 11. It is consistent with this that the air inside the COL also has reduced water vapor mixing ratios [*Schaeler et al.*, 2005]. The COL was advected from

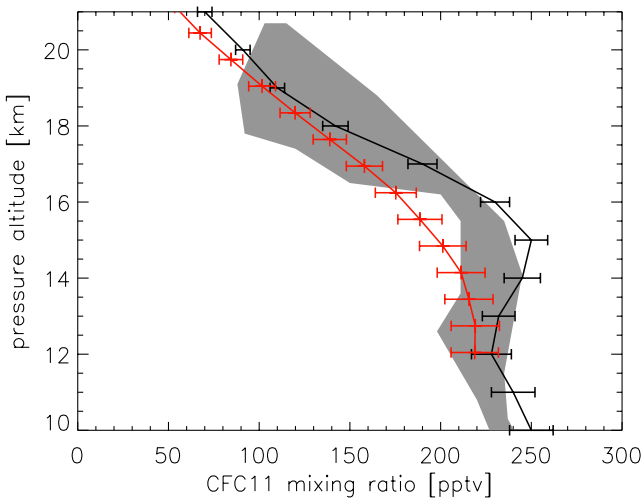

Figure 6. Comparison between CRISTA CFC 11 (red, all CRISTA data averaged over the region 62.5–72.5°N, 120–180°W), a CFC 11 profile from MkIV (black), and CFC 11 measurements from ACATS IV (envelope in grey). For details, see text.

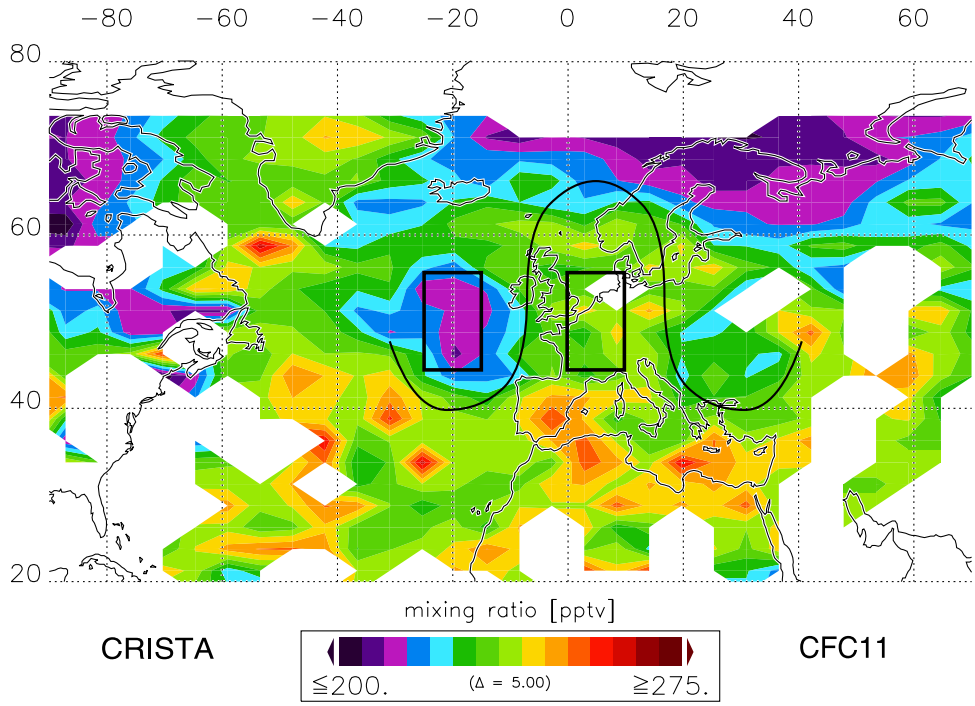

Figure 7. CFC 11 distribution at 147 hPa (≈14 km) over the TRACHT area as measured by CRISTA 2 during one day (11 August 1997, 15:00 GMT, to 12 August 1997, 15:00 GMT). To better visualize spatial structures, the observations were smoothed here applying a 200 × 400 km^2 wide averaging filter. For details, see text.

higher latitudes during the previous days. There are still remnants of a horizontal connection to higher latitudes. About 50° further east there is another but weaker structure of CFC 11-reduced air, which also belongs to the omega structure. As the temperature distribution (Figure 1) shows, the air inside the COL is significantly warmer than outside. This indicates, on the one hand, downward transport resulting in adiabatic warming. On the other hand, it shows that the air in the COL originated at higher latitudes, which are warmer during this time of the year. (Both processes act simultaneously. See section 3.4.) Figure 8 shows two mean CFC 11 profiles: one is the average of 13 vertical scans inside the COL and the other the average of 9 vertical scans outside at the same latitude. The averaging regions are marked in Figure 7 by black rectangles. Inside the COL the mean CFC 11 mixing ratio is significantly reduced. The vertical extent of the COL can be identified by means of CFC 11 from about 70 hPa down to 200 hPa, and it also shows up in water vapor mixing ratios down to 300 hPa [*Schaeler et al.*, 2005]. The reduced CFC 11 and water vapor mixing ratios are due to downward transport and to horizontal advection from higher latitudes as well (see below).

[27] The meteorological fields used for CFC 11 transport simulations (section 3.4) show that the modification of the geopotential height field by the omega block reaches up to 50 hPa, whereas the humidity distribution is only affected up to 70 hPa. The temperature field exhibits a weak wavelike signature up to 30 hPa. It should be noted that the core of the cutoff low, which contains air from higher latitudes, is warmer than its surroundings above about 300 hPa. This is mainly a consequence of the temperature increase towards the pole in the stratosphere in summer. At lower levels the cutoff low shows the usual temperature structure, namely a cold core. The dynamical tropopause (here defined as the 2-PVU surface) is found at quite low levels in the cyclonic wings of the omega structure and moved upward above normal in the central ridge. The tropopause was occasionally bent down to about 500 hPa in the COL on the western side of the ridge.

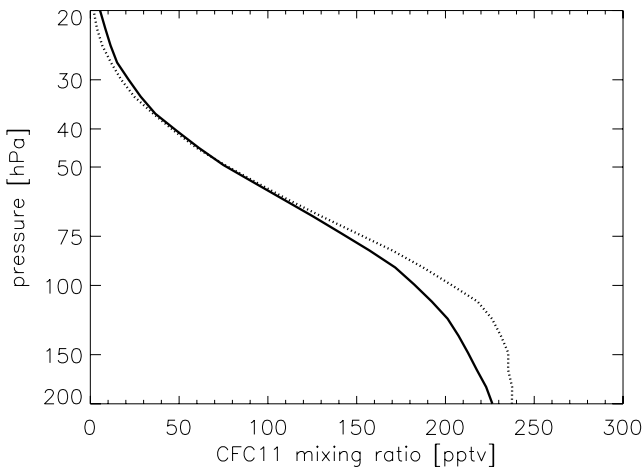

Figure 8. CFC 11 mean profiles inside the COL (solid line; averaged over 45–55°N, 15–25°W) and outside the COL (dotted line; averaged over 45–55°N, 0–10°E). Statistical errors of the mean profiles are on the order of 1 pptv (≈ line width). (Data are from 11 August 1997, 15:00 GMT, to 12 August 1997, 15:00 GMT).

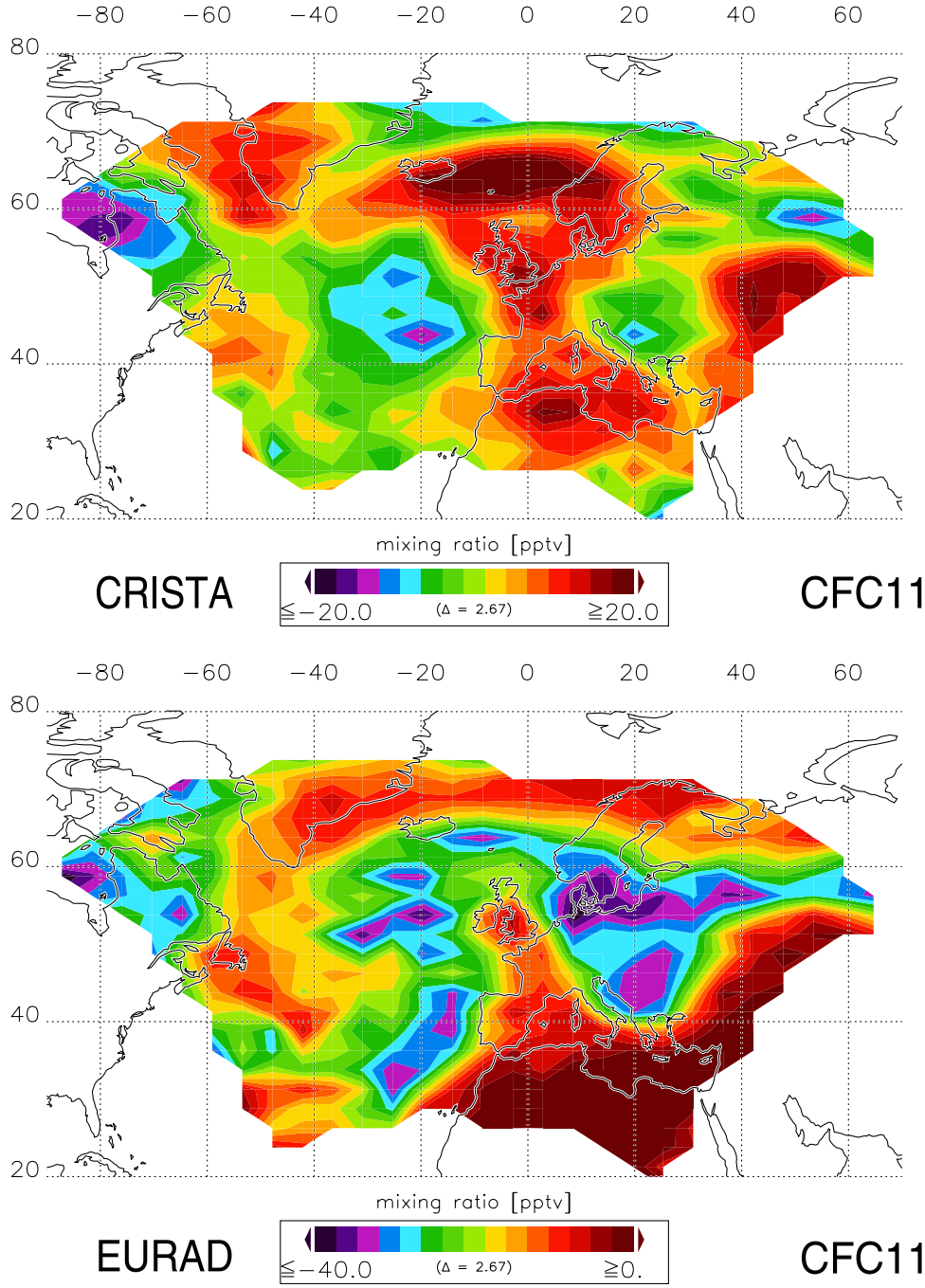

Figure 9. Detrended CFC 11 distribution at 100 hPa in the TRACHT region during the time period from 10–13 August 1997 as measured by CRISTA (upper map) and modeled by EURAD (interpolated to the CRISTA measurement grid; lower map). Both data sets are smoothed applying a 200 × 400 km^2 wide averaging filter. The EURAD data have a negative bias of about 20 pptv.

3.4. Comparison With Model Results

[28] The COL provides a good opportunity to compare the measured structures with a regional high resolution model. The TRACHT region has been simulated by the EURAD model [*Feldmann et al.*, 2003]. Since EURAD is a regional model, data for initialization as well as to fix the boundary conditions are needed. For the upper model domain we used data sets obtained from an assimilation of the CRISTA CFC 11 measurements by means of the Research for Ozone in the Stratosphere and its Evolution (ROSE) model [*Riese et al.*, 1999b, and references therein]. These data have been complemented by average (climatological) tracer profiles at lower levels. For the following analysis, the EURAD results are interpolated onto the CRISTA measuring grid in space and time. For the comparison of the structure functions discussed in section 5, the interpolated EURAD results are detrended using the zonal means of the corresponding CRISTA data. Figure 9 com-

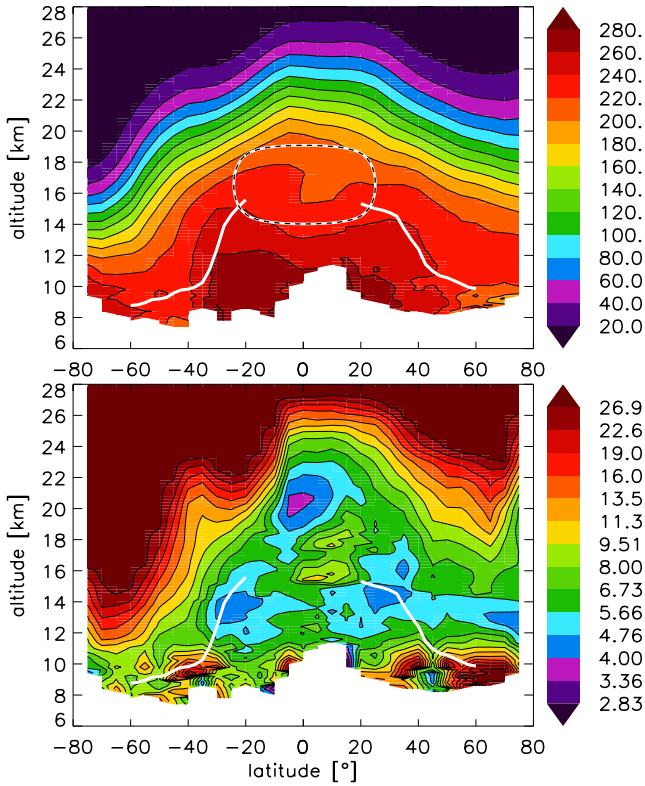

Figure 10. Altitude/latitude distribution of CFC 11 mixing ratios in pptv (top) and respective standard deviations in percent (bottom). Data are given in bins of 5° latitude × 200 m altitude for 9–13 August 1997. Altitude/latitude bins with less than five data points are left blank. Mixing ratios greater than 280 pptv are plotted in dark red, mixing ratios less than 20 pptv are plotted in dark violet. Tropopause (2.5 PVU, ECMWF) is shown as white lines. Data in encircled area are uncertain (see text).

pares detrended CRISTA and EURAD CFC 11 fields at 100 hPa. The omega structure including the COL, which is visible in the CRISTA data, is clearly reflecting the geopotential height field during the blocking event that occurred during the CRISTA 2 mission. It is well reproduced by the EURAD model. The COL and the corresponding eastern low at about 50°N, 30°E with low CFC 11 are separated by a region of high CFC 11, which extends from northern Africa through western Europe up to about 70°N in the measurements. It approximately coincides with the ridge of the omega type blocking. The region of high CFC 11, which is present in the measurements between Iceland and Scandinavia, is located somewhat further north in the model. For the blocking event shown here tracer experiments with the EURAD model revealed that an important role is played not only by the vertical but also by the horizontal transport [*Feldmann et al.*, 2003]. It should be noted that the horizontal structures in Figure 9 (also Figure 7) are relatively subtle: the difference in CFC 11 mixing ratios in the trough and ridge regions shown in Figure 8 at 100 hPa altitude are on the order of 10% only. Such a difference corresponds to an altitude difference of 1.3 km in Figure 8. Analysis of these tracer distributions is, therefore, a demanding task for measurement and model. A relative shift in height (or pressure level) may therefore contribute to the deviation between modeled and measured mixing ratios north of the blocking structure around 100 hPa. The difference is much less pronounced at lower levels. Another possible reason may be that the model slightly underestimates the meridional transport of CFC 11 rich air over Ireland towards north higher levels. Furthermore, a ridge existed during the averaging period over Newfoundland and southern Greenland according to the ECMWF analysis and the simulation with the regional model. The modeled ridge may have initiated too strong CFC 11 uplifting and transport across the Atlantic north of Iceland thus leading to higher calculated tracer mixing ratios than those observed.

[29] Despite such discrepancies it is important to note that the simulations point to significant differences with respect to meso-scale tracer transport around the tropopause in the western (COL), central (anticyclonic) and eastern (cyclonic) part of the omega flow pattern. For instance, CFC 11 rich air is lifted from lower levels to the tropopause region on the western side of the central ridge forming streamers on the northern side of the COL and the northwest side of the eastern trough thus generating smaller scale structures contributing to the spectral energy at larger horizontal wave numbers of the CFC 11 field. It is interesting to note that the simulated horizontal and vertical advective flux in the UTLS region is stronger in the eastern than in the western part of the omega structure. The reason is the higher persistence of the COL structure during the blocking event, whereas the eastern trough was characterized by high dynamical variability due to repeated tropopause fold and streamer formation.

4. Global CFC 11 Analysis

[30] Global CFC 11 fields covering the altitude range from the stratosphere down to the upper troposphere are now available from the CRISTA experiment. Figure 10 shows the global distribution of zonally averaged CRISTA CFC 11 mixing ratios and the corresponding standard deviations over the whole altitude range evaluated. The measured data have been interpolated onto a regular vertical grid with an altitude resolution of 200 m. These profiles have then been sorted into latitude bins 5° wide. The zonal mean mixing ratios are also given in Table 1 on a 10° × 1 km grid. The finer resolution in Figure 10 is given to show some fine structures in the tropics (TTL).

[31] CFC 11 is an anthropogenic product and has its only source in the troposphere. In the stratosphere, CFC 11 mixing ratios are highest in the tropics, where tropospheric air enters the stratosphere and decrease during the further transport to higher latitudes and altitudes due to photolysis. The different meridional gradients in zonal mean CFC 11 (Figure 10, higher altitudes) are due to transport barriers. During the CRISTA 2 period planetary wave activity was exceptionally high in the southern hemisphere resulting in a strong deformation of the southern polar vortex and the extraction of a streamer from the tropics [*Riese et al.*, 2002]. The strong vortex deformation shows up impressively in the high values of the CFC 11 standard deviations centered at

Table 1. Zonal Mean Mixing Ratios of CRISTA CFC11[a]

	−70°	−60°	−50°	−40°	−30°	−20°	−10°	0°	10°	20°	30°	40°	50°	60°	70°
28 km	2.6	2.1	2.2	3.0	3.0	3.8	7.1	11	11	12	7.9	4.0	3.0	3.2	3.6
27 km	2.5	2.3	2.8	4.0	4.1	6.7	15	22	21	21	15	7.2	4.4	4.0	4.6
26 km	2.5	2.7	4.2	6.4	6.8	13	29	37	35	36	26	13	7.8	6.6	7.2
25 km	2.5	3.5	6.8	12	13	24	48	57	55	54	40	22	13	10	11
24 km	2.7	5.2	12	21	23	41	74	84	80	77	58	35	23	18	18
23 km	3.1	7.9	21	35	39	64	104	114	108	103	78	51	36	28	26
22 km	3.8	12	34	55	63	93	135	145	138	129	102	74	55	43	39
21 km	4.9	19	52	79	92	127	164	172	165	154	126	99	77	61	55
20 km	7.3	29	74	106	126	160	189	195	188	176	152	129	103	85	75
19 km	12	42	97	134	159	–	–	–	–	–	176	158	131	112	98
18 km	21	60	122	161	188	–	–	–	–	–	196	185	158	141	125
17 km	38	82	145	186	213	–	–	–	–	–	214	208	184	170	154
16 km	61	106	167	206	229	–	–	–	–	–	227	223	204	193	179
15 km	92	132	185	220	240	–	–	–	–	–	235	233	219	212	201
14 km	127	157	199	228	246	–	–	–	–	–	242	238	226	221	215
13 km	161	178	209	233	252	252	250	242	245	246	249	241	228	223	222
12 km	193	202	219	236	261	263	261	252	257	253	254	247	232	224	221
11 km	216	216	228	238	266	272	274	264	–	256	259	253	234	226	221
10 km	243	236	238	234	268	272	270	–	–	265	263	237	227	218	213
9 km	244	234	236	231	276	271	270	–	–	–	269	251	242	216	185
8 km	–	241	234	236	293	–	285	–	–	–	–	–	–	–	–

[a]Data are given for altitude versus latitude. Altitude/latitude bins with less than five data points and uncertain tropical data are left blank. Volume mixing ratio units are ppt. Data are from 9–13 August 1997.

about 60°S (Figure 10). The other maximum located at about 22 km and 20°S is caused by the streamer.

[32] Below about 18 km, the general shape of the latitudinal distribution of CFC 11 mixing ratios changes: In the tropics the isopleths are almost horizontal and show even a relative minimum (“tropical trough”) near the equator. This regime is approximately the area of the TTL.

[33] The precision of the CFC 11 data is about 1–2% in the troposphere and on the order of 6% in the stratosphere. Hence all differences between adjacent color steps in Figure 10 should be significant. Typically, each latitude bin contains about 750–1000 vertical profiles. The lowermost boundary of the data field is mainly due to clouds in the CRISTA field of view. In the lowermost kilometer above this boundary the data density is 20–60 data points per bin. Considering this precision, the tropical trough structure should be real or, alternatively, indicate a systematic error in the data retrieval.

[34] An inconsistency of the data is seen, indeed, if the tropopause height is studied. The 2.5 PVU tropopause is shown as a white line in Figure 10 (following *Haynes and Shuckburgh* [2000]). There are many parts of the CFC 11 latitude distribution below the tropopause where the mixing ratios are lower than the ground value of CFC 11 (267 pptv). Many of these are well below the chemopause level (14 km), and are in disagreement with balloon and airplane measurements. Low mixing ratios can come about if too high temperatures are used in the retrieval process. (A temperature increase of 1 K means a mixing ratio decrease of 2–3%.) As pointed out above, we have used the CUC temperatures for retrieval which have the same absolute accuracy as the UKMO temperatures. A relatively small warm bias (0–1 K) has been observed at middle northern latitudes (in the TRACHT area; see section 2.2 above), which is covered by our absolute error quoted. We therefore use our maximum error of 8% and apply it to the mixing ratio of 267 pptv. A threshold value of about 245 pptv is thus obtained; values lower than this should not occur below the tropopause or chemopause. Figure 10 shows that this criterion is obeyed at middle latitudes. It is, however, violated at low latitudes (equatorward of 30°) and at high latitudes. There is suspicion that UKMO temperatures have a stronger warm bias in the tropics near the tropopause [e.g., *Read et al.*, 2004]. Figure 11 shows therefore the mean difference between 26 radiosondes launched from Cocos Island (12°S, 96.5°E) during and around the CRISTA 2 mission and corresponding UKMO temperatures. A warm bias of UKMO of about 2.5 K in the 100 hPa altitude regime is obtained. (A similar value of 1–2 K was found by *Randel et al.* [2004].) The bias suggests that the low CFC 11 mixing ratios at low latitudes are to some extent or entirely due to a warm bias of the retrieval temperatures. It implies that the trough structure may be weaker than apparent in Figure 10. To emphasize this, the trough has been encircled

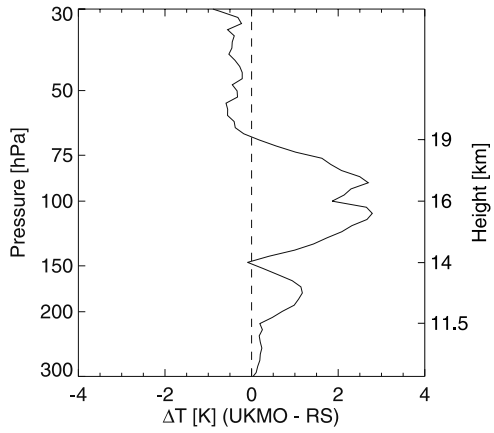

Figure 11. Mean temperature difference ΔT (UKMO minus radiosondes) at Cocos Island (12.1°S, 96.5°E). Radiosonde data are from 28 launches during 6–21 August 1997. Daily UKMO temperatures are interpolated to the location of the corresponding radiosonde profiles. Height scale in kilometers is approximate.

in Figure 10 by a dashed line. Because of its uncertainty, the trough will not be further analyzed here.

[35] The discrepancy at high latitudes is believed to be due to a very high variability of the tropopause height. This was shown by EURAD model calculations for the TRACHT area, and discussed by *Schaeler et al.* [2005, Figure 7]. Also the CFC 11 mixing ratios show very high variability (see Figure 10b and *Offermann et al.* [2003]). This suggests that mean values of the tropopause height and of the trace gas mixing ratios do not correspond to each other given such a variability [see also *Schaeler et al.*, 2005, Figures 5 and 6].

5. Discussion

[36] Structure and dynamics analyses in the upper troposphere and lower stratosphere region are frequently based on water vapor and ozone data. We here present CFC 11 from the CRISTA 2 experiment, which is an especially suitable tracer because of its steep vertical profile. Mixing ratios were retrieved by means of CUC temperatures which are a combination of CRISTA and UKMO temperatures. Mixing ratio precision is very high (1–2%) which supports dynamics analyses. Corresponding data on water vapor and ozone are presented in the companion paper of *Schaeler et al.* [2005], which also gives eddy transports of these three gases.

[37] As was mentioned above, the CFC 11 mixing ratios presented here are the first global data set at high spatial resolution which covers the upper troposphere and the lower stratosphere. We have therefore no data available to check a peculiarity that we find in the tropics: Near the equator our CFC 11 mixing ratios show a trough structure (relative minimum) near the latitudes and altitudes of the TTL. The trough is relatively flat (order of 10%) and would hardly be seen in Figure 10 if the color steps in that picture had been chosen coarser. A relatively minor change in retrieval temperature might be sufficient to make the trough disappear. The accurate knowledge of tropical tropopause (TTL) temperatures is a cumbersome problem, as they tend to depend on measurement technique. Relatively close agreement has been obtained for radiosonde, FUB analysis, and ERA 40 data by *Randel et al.* [2004]. UKMO temperatures, however, have a warm bias of 1–2 K, and NCEP re-analysis data have a warm bias of 2–3 K, following these authors. GPS temperatures appear to be close to the radiosondes (0–1 K), though positive as well as negative deviations have been obtained from two different satellites in different time intervals (GPS/CHAMP [*Schmidt et al.*, 2004] and GPS/MET [*Randel et al.*, 2003]). It is, therefore, uncertain at present which bias correction would be justified, and the trough remains an open question here.

[38] At middle northern latitudes the area of Western Europe and the Atlantic (TRACHT area) was specifically studied for meso-scale transport structures. For this purpose the CRISTA measurements were compared to simulations of the high resolution regional model EURAD. This is the first comparison of high density CFC 11 measurements and a high resolution transport (and chemistry) model, and very reasonable agreement is obtained. The investigation is mainly focusing on an outstanding feature during the CRISTA 2 mission at middle latitudes, namely a blocking event characterized by an omega circulation pattern with a highly persistent COL at its western wing. The model domain (TRACHT region) was chosen to cover the whole pattern. It should be noted that at the time of the CRISTA 2 flight significant synoptic scale dynamic activity existed in the northern hemisphere at higher middle latitudes at most longitudes in the latitude belt adjacent to the polar cap and extending from about 70 to 45 degrees, as, for instance, evident from analyses of tropopause height and potential vorticity distribution. The peculiarity of the selected domain only results from the appearance of a rather persistent blocking event.

[39] The different parts of the blocking exhibit clear differences of spatial and temporal variability of meso-scale CFC 11 transport which appears to be most intense in the UTLS of the eastern trough and less intense, but by no means weak, in the central anticyclonic part. As already mentioned streamers of CFC 11 rich air from lower levels were generated at the western flank of the ridge which contributed to the tracer budget of both cyclonic wings of the omega structure. This is an indication of mixing of tropospheric air with air from the lower stratosphere generated through the blocking event. The COL and the eastern trough with its intense tropopause folding and streamer formation are regions where downward mixing of stratospheric air into the troposphere is dominating [*Kowol-Santen et al.*, 2000]. In the eastern trough the vertical component of the advective CFC 11 flux is generally divergent at tropopause heights during the CRISTA 2 episode, indicating average downward transport of air with smaller mixing ratios from upper levels. In the COL regions alternating periods with convergent and divergent vertical CFC 11 fluxes are found.

[40] Atmospheric structures and fluctuations are thus seen on very different spatial and temporal scales. To obtain an overview on the full spectrum of fluctuations, we calculate structure functions similar to *Cho et al.* [2000]: We define the structure function of order q of a scalar quantity μ, as in our case the volume mixing ratio of CFC 11, as follows:

$$S_q(\Delta x) = \sqrt[q]{\langle |\mu(x+\Delta x) - \mu(x)|^q \rangle} \qquad (1)$$

Here $\langle \ldots \rangle$ denotes averaging over all available locations x. The spatial lag Δx is given by the measurement grid. Particularly, the second order structure function $S_2(\Delta x)$ can easily be shown to be approximated by the standard deviation of the differences $\mu(x + \Delta x) - \mu(x)$.

[41] CRISTA data are detrended by means of a linear fit to the zonal means within the latitude range from 20–70°N. The structure functions S_q (Δx) in the TRACHT region are then calculated along track for bins Δx = 0–300 km, 300–600 km, 600–900 km and so on.

[42] Figure 12 shows the structure functions of the first to fourth order for CFC 11 derived from the detrended CRISTA measurements in the TRACHT region in the time period from 10–13 August 1997 at pressure levels of 100 hPa and 147 hPa.

[43] From the Wiener-Khinchine theorem it follows that for our definition of S_2 the log-log slope (denoted here by ξ_2) is related to the log-log spectral slope β of the power spectrum $E(k) \sim k^{-\beta}$ by the function $2\xi_2 + 1 = \beta$ [*Cho et al.*, 2000] (k is the wavenumber). The two specific slopes ξ_2 corresponding to $\beta = 1$ and $\beta = 2$ are sketched in Figure 12. If scales larger than 2500 km are excluded, the log-log slope

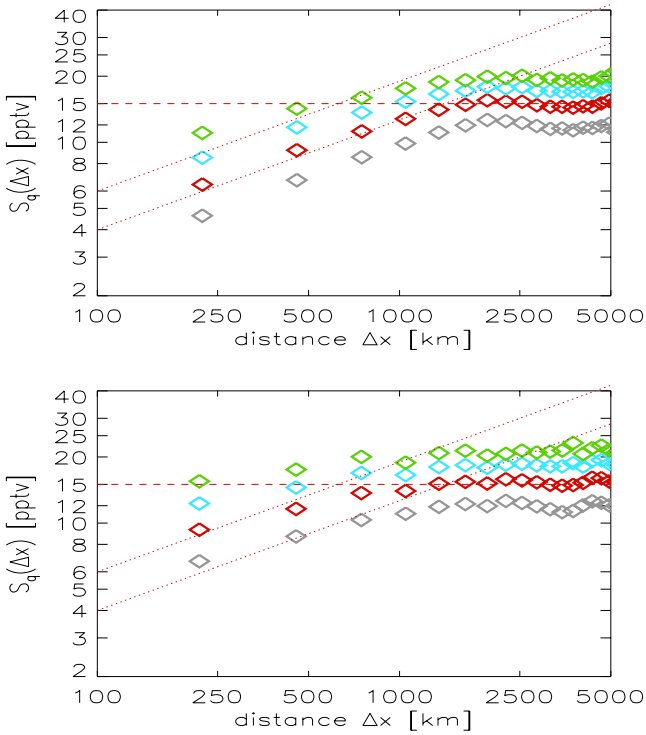

Figure 12. Structure functions of order $q = 1$ (grey), $q = 2$ (red), $q = 3$ (blue), and $q = 4$ (green) for CFC 11 measured by CRISTA 2 in the TRACHT region in the time period from 10–13 August 1997. The upper panel is for 100 hPa (≈16 km), and the lower panel is for 147 hPa (≈14 km). The lines denote log–log slopes corresponding to $\beta = 1$ (dashed) and $\beta = 2$ (dotted). For details, see text.

of the second order structure function of CRISTA CFC 11 is close to $\beta = 2$ at 100 hPa and somewhat flatter at 147 hPa. This is compatible with recent model results by *Haynes and Vanneste* [2004], who calculated tracer power spectra for realistic lower stratospheric wind fields. They found $\beta = 2$ for scales of 20–200 km and $\beta = 1$ for larger scales (order of 1000 km). *Cho et al.* [2000] analyzed water vapor data on horizontal scales of 0.1–10 km at an altitude of 7.6 km (collected by an airborne experiment) and found a value for β of about 1.8 for the free extratropical troposphere.

[44] The log-log slopes of structure functions derived from CRISTA CFC 11 tend to decrease with increasing order, e.g. when comparing the fourth to the first order. A similar so-called anomalous scaling behavior of the structure functions equivalent to a multifractal tracer field has been found for water vapor [*Cho et al.*, 2000] and ozone [*Cho et al.*, 2001]. This results from a significant intermittency and roughness of the respective tracer field, which would not have been expected in the case of smooth advection and diffusion [*Cho et al.*, 2001].

[45] Figure 13 compares the second order structure functions derived from detrended CRISTA measurements and detrended EURAD results for the whole model region at 100 hPa and 147 hPa. At the two altitudes the structure functions derived from modeled CFC 11 results agree relatively well with the measurements. This means that the variability in the model is comparable to the measured variability on all scales. These results are further used in our companion paper by *Schaeler et al.* [2005]. In that paper, EURAD CFC 11 structure functions are used to derive atmospheric correlation lengths and correlation times. These are used to estimate eddy diffusion coefficients, which in turn are compared to measured eddy coefficients.

6. Summary and Conclusions

[46] Two new data products from the CRISTA 2 mission (August 1997) are presented in the altitude regime 8–20 km: CUC temperatures and CFC 11 mixing ratios.

[47] CRISTA temperature measurements are combined with UKMO temperatures. This yields a data set with the absolute accuracy of UKMO and the high precision and high spatial resolution of CRISTA. These CRISTA-UKMO-Combined (CUC) temperatures are compared to in situ measurements of radiosondes and airplanes. Close agreement is obtained (<1 K) except at scales that are below the resolution of a limb scanning measurement (250 km). At tropical latitudes (TTL area), however, the data are relatively uncertain.

[48] CRISTA CFC 11 mixing ratios are the first near global data set at high spatial resolution in this altitude regime. They were retrieved by means of the CUC temperatures. The CFC 11 data have been compared to suborbital measurements (balloons and airplane) and very good agreement is obtained at middle latitudes. CFC 11 is particularly interesting as a tracer for dynamical structures because of its

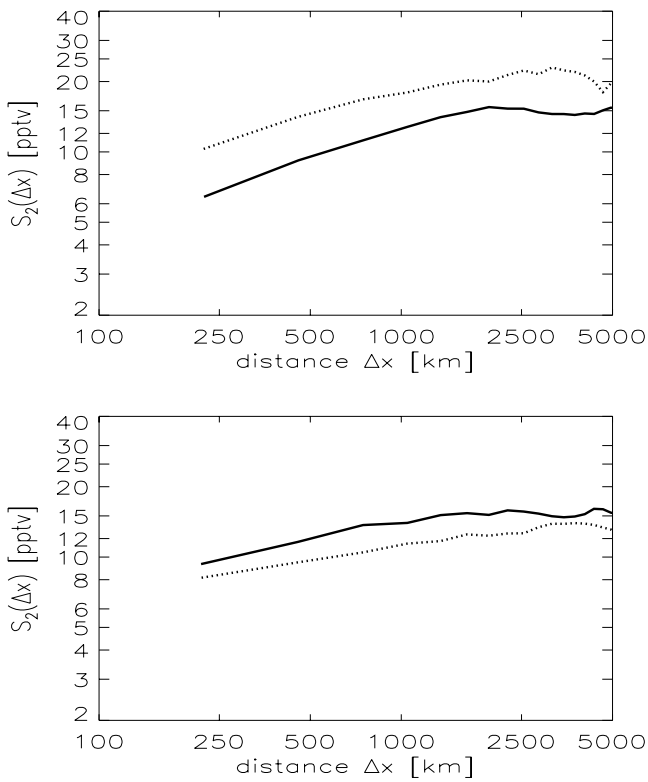

Figure 13. Second-order structure functions of CFC 11 in the TRACHT region during the time period from 10–13 August 1997 at 100 hPa (top) and 147 hPa (bottom): CRISTA measurements (solid lines) and EURAD results (dotted lines).

simple photochemistry and steep vertical profile. The precision of the CFC 11 data is very high (1–2% at the lower altitudes) because of the good signal/noise ratio of the CRISTA measurements.

[49] We have used the CUC temperatures and CFC 11 mixing ratios in a regional and in a global analysis. The regional analysis was performed over the north Atlantic and western Europe area (''TRACHT area''). Because of the high CRISTA data density it reveals considerable dynamical structures here such as an omega structure with a cutoff low (COL). These are visible in both the CUC temperatures and the CFC 11 mixing ratios. They indicate substantial vertical and horizontal transport. These transports and other details have been analyzed by means of a high resolution regional chemical transport model (EURAD). CUC temperatures, mixing ratios of CFC 11, water vapor, and ozone have been used to check on the EURAD model in the TRACHT region [see also *Schaeler et al.*, 2005]. This is the first comparison of a data set taken from space with a spatial resolution this high, and a high resolution transport model. The EURAD model is found to reproduce the measured prominent structures reasonably well. Simulation of detailed features of the experimental CFC 11 fields may be hampered by the fact that CRISTA and model heights may slightly differ. The appearance of an omega blocking system during the mission enabled a comprehensive analysis, the first of its kind, regarding the impact of such an event on tracer transport with the possibility of model evaluation [*Feldmann et al.*, 2003]. Differences with respect to transport behaviour in the three parts of the omega structure could be identified with the help of the simulations. The western wing containing the COL appeared to be dynamically less variable than the eastern cyclonic part which therefore exhibited more efficient meso-scale transport. And the central ridge caused polluted lower level air from the south to penetrate to tropopause levels in the north.

[50] A scaling analysis by means of structure functions has been performed to study the atmospheric fluctuations by means of CFC 11 values measured by CRISTA as well as those computed by EURAD. The gradients of the measured second order structure functions agree well with recent results published in the literature. The corresponding structure functions of EURAD agree well with the measured ones, which means that EURAD reproduces well the variability of the CFC 11 field in the TRACHT area. First to fourth order structure functions suggest multifractal behavior of the measured CFC 11 field in the upper troposphere and lower stratosphere in the TRACHT region. This is also in agreement with the recent literature.

[51] In the global analysis we observe a peculiarity near the equator. The CFC 11 mixing ratios show a relative minimum (''trough'') near the TTL region. This minimum might be an artifact produced by a warm bias of the UKMO temperatures as it is presently discussed in the literature. A respective bias was also seen in a set of radiosonde measurements around the time of the CRISTA flight. As we have no accurate retrieval temperatures at present the detailed nature of the trough remains an open question here.

[52] **Acknowledgments.** The authors thank X. Tie (NCAR, Boulder, Colorado, USA) for providing the ROSE model. Cocos Island radiosonde data were obtained from the Australian National Climate Centre, Data Services, Bureau of Meteorology. ECMWF analyses have been employed for the EURAD model with kind agreement by the German Weather Service (DWD). ECMWF ERA 40 data have been obtained from the ECMWF data server. The CRISTA experiment is funded by grant 50 QV 9802 4 of the Bundesministerium fuer Bildung und Forschung (BMBF, Bonn) through the Deutsches Zentrum fuer Luft- und Raumfahrt (DLR, Bonn). The TRACHT project was funded by BMBF under grant 07ATF06. We thank the two referees for their helpful comments and suggestions.

References

Ancellet, G. M., M. Beekmann, and A. Papyannis (1994), Impact of a cutoff low development on downward transport of ozone in the troposphere, *J. Geophys. Res.*, *99*, 3451–3468.

Appenzeller, C., and H. C. Davies (1992), Structure of stratospheric intrusions into the troposphere, *Nature*, *358*, 570–572.

Benzi, R., B. Saltzman, and A. Wiin-Nielsen (Eds.) (1986), *Anomalous Atmospheric Flows and Blocking*, *Adv. Geophys.*, vol. 29, 459 pp., Elsevier, New York.

Bingham, G. E., D. K. Zhou, B. Y. Bartschi, G. P. Anderson, D. R. Smith, J. H. Chetwynd, and R. M. Nadile (1997), Cryogenic Infrared Radiance Instrumentation for Shuttle (CIRRIS 1A) earth limb spectral measurements, calibration, and atmospheric O_3, HNO_3, CFC-12, and CFC-11 profile retrieval, *J. Geophys. Res.*, *102*, 3547–3558.

Chang, A. Y., et al. (1996), A comparison of measurements from ATMOS and instruments aboard the ER-2 aircraft: Halogenated gases, *Geophys. Res. Lett.*, *23*, 2393–2396.

Cho, J. Y. N., R. E. Newell, and G. W. Sachse (2000), Anomalous scaling of mesoscale tropospheric humidity fluctuations, *Geophys. Res. Lett.*, *27*, 377–380.

Cho, J. Y. N., V. Thouret, R. E. Newell, and A. Marenco (2001), Isentropic scaling analysis of ozone in the upper troposphere and lower stratosphere, *J. Geophys. Res.*, *106*(D9), 10,023–10,038.

Ebel, A., H. Hass, H. J. Jakobs, M. Memmesheimer, M. Laube, A. Oberreuter, H. Geiss, and Y.-H. Kuo (1991), Simulation of ozone intrusion caused by a tropopause fold and a cutoff low, *Atmos. Environ., Part A*, *25*, 2131–2144.

Elbern, H., J. Kowol, R. Sladkovic, and A. Ebel (1997), Deep stratospheric intrusions: A statistical assessment with model guided analyses, *Atmos. Environ.*, *31*, 3207–3226.

Elbern, H., J. Hendricks, and A. Ebel (1998), A climotology of tropopause folds by global analyses, *Theor. Appl. Climotol.*, *59*, 181–200.

Elkins, J. W., T. M. Thompson, T. H. Swanson, J. H. Butler, B. D. Hall, S. O. Cummings, D. A. Fisher, and A. G. Raffo (1993), Decrease in the growth rates of atmospheric chlorofluorocarbons 11 and 12, *Nature*, *364*, 780–783.

Elkins, J. W., et al. (1996), Airborne gas chromatograph for in situ measurements of long-lived species in the upper troposphere and lower stratosphere, *Geophys. Res. Lett.*, *23*, 347–350.

Engel, A., U. Schmidt, and R. A. Stachnik (1997), Partitioning between chlorine reservoir species deduced from observations in the Arctic winter stratosphere, *J. Atmos. Chem.*, *27*, 107–126.

Engel, A., M. Strunk, M. Mueller, H.-P. Haase, C. Poss, I. Levin, and U. Schmidt (2002), Temporal development of total chlorine in the high-latitude stratosphere based on reference distributions of mean age derived from CO_2 and SF_6, *J. Geophys. Res.*, *107*(D12), 4136, doi:10.1029/2001JD000584.

Fabian, P., and R. Borchers (2001), Growth of halocarbon abundances in the stratosphere between 1977 and 1999, *Adv. Space Res.*, *28*(7), 961–964.

Feldmann, H., A. Ebel, D. Offermann, B. Schaeler, and V. Kuell (2003), Final report on the project TRACHT-MODEL, Rhen. Inst. Environ. Res., Cologne and Univ. of Wuppertal, Wuppertal, Germany. (Available at http://www.eurad.uni-koeln.de/TRACHT)

Folkins, I., M. Loewenstein, J. Podolske, S. J. Oltmans, and M. Proffitt (1999), A barrier to vertical mixing at 14 km in the tropics: Evidence from ozonesondes and aircraft measurements, *J. Geophys. Res.*, *104*, 22,095–22,102.

Folkins, I., C. Braun, A. M. Thompson, and J. Witte (2002), Tropical ozone as an indicator of deep convection, *J. Geophys. Res.*, *107*(D13), 4184, doi:10.1029/2001JD001178.

Fournier, A. (2003), Atmospheric energetics in the wavelet domain. Part II: Time-averaged observed atmospheric blocking, *J. Atmos. Sci.*, *60*, 319–338.

Fujiwara, M., M. K. Yamamoto, H. Hashiguchi, T. Horinouchi, and S. Fukao (2003), Turbulence at the tropopause due to breaking Kelvin waves observed by the Equatorial Atmosphere Radar, *Geophys. Res. Lett.*, *30*(4), 1171, doi:10.1029/2002GL016278.

Grell, G., J. Duddhia, and D. Staufer (1995), A description of the fifth-generation Penn State/NCAR meso-scale model (MM5), *Tech. Note NCAR/TN-398+STR*, Natl. Cent. for Atmos. Res., Boulder, Colo.

Grossmann, K. U., D. Offermann, O. Gusev, J. Oberheide, M. Riese, and R. Spang (2002), The CRISTA-2 mission, *J. Geophys. Res.*, *107*(D23), 8173, doi:10.1029/2001JD000667.

Haynes, P. H., and E. Shuckburgh (2000), Effective diffusivity as a diagnostic of atmospheric transport: 2. Troposphere and lower stratosphere, *J. Geophys. Res.*, *105*, 22,795–22,810.

Haynes, P. H., and J. Vanneste (2004), Stratospheric tracer spectra, *J. Atmos. Sci.*, *61*, 161–178.

Heese, B., S. Godin, and A. Hauchecorne (2001), Forecast and simulation of stratospheric ozone filaments: A validation of a high-resolution potential vorticity advection model by airborne ozone lidar measurements in winter 1998/1999, *J. Geophys. Res.*, *106*(D17), 20,011–20,024.

Helten, M., H. G. J. Smit, W. Straeter, D. Kley, P. Nedelec, M. Zoeger, and R. Busen (1998), Calibration and performance of automatic compact instrumentation for the measurement of relative humidity from passenger aircraft, *J. Geophys. Res.*, *103*, 25,643–25,652.

Holton, J. R., P. H. Haynes, M. E. McIntyre, A. R. Douglass, R. B. Rood, and L. Pfister (1995), Stratosphere–troposphere exchange, *Rev. Geophys.*, *33*, 403–439.

Kowol-Santen, J., H. Elbern, and A. Ebel (2000), Estimation of cross-tropopause air mass fluxes at midlatitudes: Comparison of different numerical methods and meteorological situations, *Mon. Weather Rev.*, *128*, 4045–4057.

Lait, L. R., et al. (2002), Ozone loss from quasi-conservative coordinate mapping during the 1999–2000 SOLVE/THESEO 2000 campaigns, *J. Geophys. Res.*, *107*(D20), 8274, doi:10.1029/2001JD000998.

Lehmacher, G., and D. Offermann (1997), CRISTA/MAHRSI Campaign 2 Handbook, technical report, Wuppertal Univ., Wuppertal, Germany.

Luers, J. K., and R. E. Eskridge (1998), Use of radiosonde temperature data in climate studies, *J. Clim.*, *11*, 1002–1019.

Manney, G. L., R. Swinbank, S. T. Massie, M. E. Gelman, A. J. Miller, R. Nagatani, A. O'Neill, and R. W. Zurek (1996), Comparison of UK Meteorological Office and U.S. National Meteorological Center stratospheric analyses during northern and southern winter, *J. Geophys. Res.*, *101*, 10,311–10,334.

Marenco, A., et al. (1998), Measurement of ozone and water vapor by Airbus in-service aircraft: The MOZAIC airborne program, An overview, *J. Geopyhs. Res.*, *103*, 25,631–25,642.

Memmesheimer, M., J. Tippke, A. Ebel, H. Hass, H. J. Jakobs, and M. Laube (1991), On the use of EMEP emission inventories for European scale air pollution modelling with the EURAD model, paper presented at Workshop on Photo-Oxidant Modelling for Long-Range Transport in Relation to Abatement Strategies, Eur. Monit. Eval. Programme, Berlin, Germany, April.

Montzka, S. A., J. H. Butler, J. W. Elkins, T. M. Thompson, T. H. Swanson, A. D. Clarke, and L. T. Lock (1999), Present and future trends in the atmospheric burden of ozone-depleting halogens, *Nature*, *398*, 690–694.

Offermann, D., K. U. Grossmann, P. Barthol, P. Knieling, M. Riese, and R. Trant (1999), CRyogenic Infrared Spectrometers and Telescopes for the Atmosphere (CRISTA) experiment and middle atmosphere variability, *J. Geophys. Res.*, *104*, 16,311–16,325.

Offermann, D., V. Kuell, B. Schaeler, M. Jarisch, H. Claude, H. G. J. Smit, A. Ebel, and H. Feldmann (2003), Final report on Project "TRACHT-Data", technical report, Wuppertal Univ., Wuppertal, Germany. (Available at http://www.crista.uni-wuppertal.de)

Pelly, J. L., and B. J. Hoskins (2003), A new perspective on blocking, *J. Atmos. Sci.*, *60*, 743–755.

Plumb, I. C., P. F. Vohralik, and K. R. Ryan (1999), Normalization of correlations for atmospheric species with chemical loss, *J. Geophys. Res.*, *104*, 11,723–11,732.

Preusse, P., A. Doernbrack, S. D. Eckermann, M. Riese, B. Schaeler, J. Bacmeister, D. Broutman, and K. U. Grossmann (2002), Space based measurements of stratospheric mountain waves by CRISTA: 1. Sensitivity, analysis method, and a case study, *J. Geophys. Res.*, *107*(D23), 8178, doi:10.1029/2001JD000699.

Randel, W. J., F. Wu, and W. R. Rios (2003), Thermal variability of the tropical tropopause region derived from GPS/MET observations, *J. Geophys. Res.*, *108*(D1), 4024, doi:10.1029/2002JD002595.

Randel, W. J., et al. (2004), The SPARC intercomparison of middle-atmosphere climatologies, *J. Clim.*, *17*, 986–1003.

Read, W. G., D. L. Wu, J. W. Waters, and H. C. Pumphrey (2004), Dehydration in the tropical tropopause layer: Implications from the UARS Microwave Limb Sounder, *J. Geophys. Res.*, *109*, D06110, doi:10.1029/2003JD004056.

Rex, D. F. (1950), Blocking action in the middle troposphere and its effect upon regional climate. I. An aerological study of blocking action, *Tellus*, *2*, 275–301.

Riese, M., R. Spang, P. Preusse, M. Ern, M. Jarisch, D. Offermann, and K. U. Grossmann (1999a), CRyogenic Infrared Spectrometers and Telescopes for the Atmosphere (CRISTA) data processing and atmospheric temperature and trace gas retrieval, *J. Geophys. Res.*, *104*, 16,349–16,367.

Riese, M., X. Tie, G. P. Brasseur, and D. Offermann (1999b), Three-dimensional simulations of stratospheric trace gas distributions measured by CRISTA, *J. Geophys. Res.*, *104*, 16,419–16,435.

Riese, M., G. L. Manney, J. Oberheide, X. Tie, R. Spang, and V. Kuell (2002), Stratospheric transport by planetary wave mixing as observed during CRISTA-2, *J. Geophys. Res.*, *107*(D23), 8179, doi:10.1029/2001JD000629.

Roche, A. E., R. W. Nightingale, J. B. Kumer, J. L. Mergentaler, C. H. Jackman, and E. L. Fleming (1998), Distribution and seasonal variation of CFCs in the stratosphere: Comparison of satellite global data and a 2-D model, *Adv. Space Res.*, *21*, 1383–1391.

Saraf, N., G. Beig, and M. Schultz (2003), Tropospheric distribution of ozone and its precursors over the tropical Indian Ocean, *J. Geophys. Res.*, *108*(D20), 4636, doi:10.1029/2003JD003521.

Sausen, R. (1995), Analysis of blocking events from observations and ECHAM model simulations, *Tellus, Ser. A*, *47*, 421–438.

Schaeler, B., D. Offermann, V. Kuell, M. Jarisch, H. Feldmann, and A. Ebel (2005), Regional and global trace gas distributions and inferred transports in the upper troposphere and lower stratosphere, *J. Geophys. Res.*, *110*, D09104, doi:10.1029/2004JD004994.

Schmidt, T., J. Wickert, G. Beyerle, and C. Reigber (2004), Tropical tropopause parameters derived from GPS radio occultation measurements with CHAMP, *J. Geophys. Res.*, *109*, D13105, doi:10.1029/2004JD004566.

Schmidt, U., G. Kulessa, E. Klein, E.-P. Roeth, P. Fabian, and R. Borchers (1987), Intercomparison of balloon-borne cryogenic whole air samplers during the MAP/GLOBUS 1983 campaign, *Planet. Space Sci.*, *35*, 647–656.

Shepherd, T. G. (2002), Issues in stratosphere–troposphere coupling, *J. Meteorol. Soc. Jpn.*, *80*, 769–792.

Sherwood, S. C., and A. E. Dessler (2000), On the control of stratospheric humidity, *Geophys. Res. Lett.*, *27*, 2513–2516.

Sherwood, S. C., and A. E. Dessler (2001), A model for transport across the tropical tropopause, *J. Atmos. Sci.*, *58*, 765–779.

Sprenger, M., M. C. Maspoli, and H. Wernli (2003), Tropopause folds and cross-tropopause exchange: A global investigation based upon ECMWF analyses for the time period March 2000 to February 2001, *J. Geophys. Res.*, *108*(D12), 8518, doi:10.1029/2002JD002587.

Stockwell, W. R., F. Kirchern, and M. Kuhn (1997), A new mechanism for regional atmospheric chemistry modelling, *J. Geophys. Res.*, *102*(D22), 25,847–25,879.

Swinbank, R., and A. O'Neill (1994), A stratosphere–troposphere data assimilation system, *Mon. Weather Rev.*, *122*, 686–702.

Toon, G. C., et al. (1999), Comparison of MkIV balloon and ER-2 aircraft measurements of atmospheric trace gases, *J. Geophys. Res.*, *104*, 26,779–26,790.

Tuck, A. F., et al. (2004), Horizontal variability 1–2 km below the tropical tropopause, *J. Geophys. Res.*, *109*, D05310, doi:10.1029/2003JD003942.

Voemel, H., et al. (2002), Balloon-borne observations of water vapor and ozone in the tropical upper troposphere and lower stratosphere, *J. Geophys. Res.*, *107*(D14), 4210, doi:10.1029/2001JD000707.

Waugh, D. W., and B. M. Funatsu (2003), Intrusions into the tropical upper troposphere: Three-dimensional structure and accompanying ozone and OLR distributions, *J. Atmos. Sci.*, *60*, 637–653.

Waugh, D. W., and L. M. Polvani (2000), Climatology of intrusions into the tropical upper troposphere, *Geophys. Res. Lett.*, *27*, 3857–3860.

Yagi, S., A. Mita, and N. Inoue (1996), WMO International Radiosonde Intercomparison, Phase IV, (Tsukuba, Japan, 1993), in *Instruments and Observing Methods*, *WMO/TD 742*, World Meteorol. Org., Geneva.

H. Claude, Meteorological Observatory, D-82383 Hohenpeissenberg, Germany.

A. Ebel and H. Feldmann, Rhenish Institute for Environmental Research, University of Cologne, D-50931 Cologne, Germany.

A. Engel, Institute for Meteorology and Geophysics, University of Frankfurt, D-60325 Frankfurt, Germany.

M. Jarisch and D. Offermann, Physics Department, University of Wuppertal, D-42097 Wuppertal, Germany. (jarisch@uni-wuppertal.de)

V. Kuell, Meteorological Institute, University of Bonn, D-53121 Bonn, Germany. (volker.kuell@uni-bonn.de)

B. Schaeler, CETEQ, Lise-Meitner-Str. 5-9, D-42119 Wuppertal, Germany.

H. G. J. Smit, ICG–2, Research Center Juelich, D-52425 Juelich, Germany.